Journal of Porphyrins and Phthalocyanines
J. Porphyrins Phthalocyanines 2014; **18**: 1–14
DOI: 10.1142/S1088424614501119

Published at http://www.worldscinet.com/jpp/

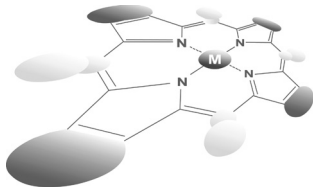

Spectroelectrochemical characterization of *meso* triaryl-substituted Mn(IV), Mn(III) and Mn(II) corroles. Effect of solvent and oxidation state on UV-visible spectra and redox potentials in nonaqueous media

Bingbing Gao[a], Zhongping Ou*[a◊], Xueyan Chen[a], Shi Huang[a], Bihong Li[a], Yuanyuan Fang[b◊◊] and Karl M. Kadish*[b◊]

[a] *School of Chemistry and Chemical Engineering, Jiangsu University, Zhenjiang 212013, China*
[b] *Department of Chemistry, University of Houston, Houston, TX 77204-5003, USA*

Received 7 September 2014
Accepted 21 September 2014

ABSTRACT: Two series of substituted manganese triarylcorroles were synthesized and characterized as to their electrochemical and spectroelectrochemical properties in CH_2Cl_2, CH_3CN and pyridine. The investigated compounds are represented as $(YPh)_3CorMn^{III}$ and $(YPh)_3CorMn^{IV}Cl$, where Cor is a trianion of the corrole and Y is a Cl, F, H or CH_3 *para*-substituent on the three phenyl rings of the macrocycle. Each neutral Mn(III) corrole exists as a four-coordinate complex in CH_2Cl_2 and CH_3CN and as a five-coordinate species in pyridine. $(YPh)_3CorMn^{III}$ undergoes two oxidations to stepwise generate a Mn(IV) corrole and a Mn(IV) π-cation radical. It also undergoes one reduction to generate a Mn(II) corrole in CH_2Cl_2 or CH_3CN. In contrast, the reduction of $(YPh)_3CorMn^{III}$ leads to a Mn(III) corrole π-anion radical in pyridine. One oxidation is observed for $(YPh)_3CorMn^{IV}Cl$ in CH_2Cl_2 and CH_3CN to generate a Mn(IV) corrole π-cation radical while Mn(III) and Mn(II) corroles are stepwise formed after reduction of the same compound. The second reduction of $(YPh)_3CorMn^{IV}Cl$ in pyridine gives a Mn(III) π-anion radical as opposed to a Mn(II) corrole with an unreduced π-ring system. The neutral, reduced and oxidized forms of each corrole were characterized by electrochemistry and UV-visible spectroelectrochemistry and comparisons are made between the UV-visible spectra and redox potentials of the compounds in different central metal oxidation states. An overall reduction/oxidation mechanism in the three solvents is proposed.

KEYWORDS: manganese(IV) and manganese(III) corroles, synthesis, electrochemistry, spectroelectrochemistry, effect of solvent and oxidation state.

INTRODUCTION

Manganese corroles have attracted much interest [1–11] due to their possible applications in the fields of catalysis [12–17], ion-selective electrodes [18], single-chain magnets [19] and medicine [20, 21]. The oxidation state of the central metal ion in manganese corroles can vary from +3 to +6 [8]. The formal oxidation state of the four-coordinate compound is +3 while the five-coordinate complex with a single anionic or σ-bonded axial ligand is assigned as having a formal metal oxidation state of +4. Six-coordinate manganese corroles have also been characterized with central metal ion oxidation states of +5 and +6 [1, 2, 6, 8].

There have been numerous electrochemical studies of Mn(III) corroles [8–12, 22, 23], but only two papers have been published on the electrochemistry of stable Mn(IV) corroles [9, 24] and no systematic comparisons have

[◊]SPP full and [◊◊] student member in good standing

*Correspondence to: Zhongping Ou, email: zpou2003@yahoo.com, tel: +86 511-88791800, fax: +86 0511-88791800; Karl M. Kadish, email: kkadish@uh.edu, tel: +1 (713) 743-2740, fax: +1 (713) 743-2745

been made between the redox potentials and spectra of neutral, reduced and oxidized triaryl-substituted Mn(III) and Mn(IV) corroles containing the same series of electron-donating or electron-withdrawing substituents on the macrocycle.

This is done in the present paper which examines two series of substituted triarylcorroles containing Mn(III) and Mn(IV) as the central metal ion. The first series of compounds is represented as $(YPh)_3CorMn^{III}$ and the second as $(YPh)_3CorMn^{IV}Cl$, where Cor is a trianion of the corrole and Y is a Cl, F, H or CH_3 substituent on the *para*-position of each phenyl ring of the macrocycle. The structures of these corroles are shown in Chart 1. The neutral, reduced and oxidized forms of each manganese corrole were electrochemically and spectroscopically examined in CH_2Cl_2, CH_3CN and pyridine containing 0.1 M TBAP and a comparison is then made between the UV-visible spectra and redox potentials for each complex generated in a given oxidation state by chemical synthesis or by electrogeneration under the application of an applied oxidizing or reducing potential.

EXPERIMENTAL

Chemicals

Dichloromethane (CH_2Cl_2) was dried over molecular sieves (4 Å), stored under argon and distilled over CaH_2 prior to use. Acetonitrile (CH_3CN) was purchased from Aldrich Chemical Co., distilled over P_2O_5 under vacuum prior to use. Anhydrous pyridine (99.8%) from Sinopharm Chemical Reagent Co. or Aldrich Chemical Co., was used without further purification. Tetra-*n*-butyl ammonium perchlorate (TBAP) was purchased from Sigma Chemical or Fluke Chemika Co., recrystallized from ethyl alcohol and dried under vacuum at 40 °C for at least one week prior to use.

Instrumentation

Cyclic voltammetry was carried out at 298 K using a CHI-730E Electrochemistry Workstation. A homemade three-electrode cell was used for cyclic voltammetric measurements and consisted of glassy carbon work electrode, a platinum counter electrode and a homemade saturated calomel reference electrode (SCE). The SCE is separated from the bulk of the solution by a fritted glass bridge of low porosity which contained the solvent/supporting electrolyte mixture.

Thin-layer UV-visible spectroelectrochemical experiments were performed with a home-built thin-layer cell which has a light transparent platinum networking electrode. Potentials were applied and monitored with an EG&G PAR Model 173 potentiostat or BiStat electrochemistry station. Time-resolved UV-vis spectra were recorded with a Hewlett-Packard Model 8453 diode array spectrophotometer. High purity N_2 were used to deoxygenate the solution and kept over the solution during each electrochemical and spectroelectrochemical experiment.

MALDI-TOF mass spectra were taken on a Bruker BIFLEX III ultra-high resolution instrument using alpha-cyano-4-hydroxycinnamic acid as the matrix and the spectra obtained for examined corroles are shown in Figs S1–S8 (Supporting information). Infrared spectra were recorded with a Nicolet Nexus 470 IR spectrometer.

Synthesis

Mn(III) corroles 1–4. The corresponding free-base corroles (~40 mg, 64 mmol) were synthesized according to procedure described in literature [25] and dissolved in 30 mL *N*,*N*′-dimethylformamide containing 5 equivalents of $Mn(OAc)_2{\cdot}4H_2O$. The solution was heated to reflux under N_2 for 10 min and then cooled to room temperature, after which it was diluted by $CHCl_3$ and washed thoroughly with aqueous Na_2CO_3 to remove DMF. The organic layer was collected and dried with

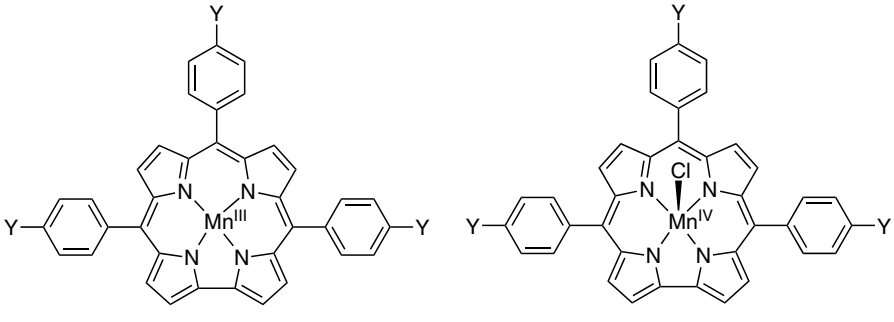

Y = Cl, $(ClPh)_3CorMn$ **1**
Y = F, $(FPh)_3CorMn$ **2**
Y = H, $(Ph)_3CorMn$ **3**
Y = CH_3, $(CH_3Ph)_3CorMn$ **4**

Y = Cl, $(ClPh)_3CorMnCl$ **5**
Y = F, $(FPh)_3CorMnCl$ **6**
Y = H, $(Ph)_3CorMnCl$ **7**
Y = CH_3, $(CH_3Ph)_3CorMnCl$ **8**

Chart 1. Structures of investigated Mn(III) and Mn(IV) triarylcorroles

anhydrous $MgSO_4$. The solvent was then removed and the residue chromatographed on neutral alumina (200–300 mesh) using CH_2Cl_2/hexane or CH_2Cl_2 as eluent. The green fraction was collected and evaporated to dryness.

$(ClPh)_3CorMn^{III}$ 1. 35 mg, yield 14%. IR (KBr): ν, cm^{-1} 3092, 2919, 1642, 1586, 1490, 1382, 1299, 1217, 1087, 1050, 1018, 801, 714, 492. UV-vis (CH_3CN): λ_{max}, nm (log ε) 405 (4.61), 433 (4.58), 654 (4.00). MS (MALDI-TOF): *m/z* calcd. for $C_{37}H_{20}N_4Cl_3Mn$: 681.879; found 679.314.

$(FPh)_3CorMn^{III}$ 2. 37 mg, yield 14.5%. IR (KBr): ν, cm^{-1} 3102, 2922, 1644, 1595, 1506, 1460, 1368, 1298, 1224, 1154, 1053, 807, 719, 606, 523. UV-vis (CH_3CN): λ_{max}, nm (log ε) 402 (4.69), 431 (4.60), 650 (4.10). MS (MALDI-TOF): *m/z* calcd. for $C_{37}H_{20}N_4F_3Mn$ 632.515; found 631.370.

Ph_3CorMn^{III} 3. 39 mg, yield 15%. IR (KBr): ν, cm^{-1} 3049, 2920, 1635, 1590, 1503, 1454, 1299, 1217, 1170, 1060, 1024, 786, 707. UV-vis (CH_3CN): λ_{max}, nm (log ε) 403 (4.51), 431 (4.47), 656 (3.98). MS (MALDI-TOF): *m/z* calcd. for $C_{37}H_{23}N_4Mn$ 578.543; found 577.583.

$(CH_3Ph)_3CorMn^{III}$ 4. 41 mg, yield 16%. IR (KBr): ν, cm^{-1} 3017, 2918, 2854, 1595, 1509, 1451, 1367, 1300, 1263, 1217, 1179, 1054, 1024, 799, 713. UV-vis (CH_3CN): λ_{max}, nm (log ε) 404 (4.29), 438 (4.30), 657 (3.74). MS (MALDI-TOF): *m/z* calcd. for $C_{40}H_{29}N_4Mn$ 620.623; found 619.389.

Mn(IV) corroles 5–8. The manganese(III) corroles (15 mg for compounds **1–3**, 20 mg for compound **4**) were dissolved in chloroform or dichloromethane and then washed with a 10% HCl solution. After the color of the solution changed from green to brownish yellow, the organic layer was collected and evaporated to dryness. The residue was dissolved in CH_2Cl_2 and chromatographed using silica gel ($CHCl_3$ as eluent). The brown-yellow fraction corresponding to the Mn(IV) corrole was collected and evaporated to dryness.

$(ClPh)_3CorMn^{IV}Cl$ 5. 13.6 mg, yield 90%. IR (KBr): ν, cm^{-1} 3095, 2922, 2853, 1588, 1486, 1352, 1300, 1165, 1089, 1054, 1022, 803, 721, 492. UV-vis (CH_3CN): λ_{max}, nm (log ε) 313 (4.39), 363 (4.48), 431 (4.70). MS (MALDI-TOF): *m/z* calcd. for $C_{37}H_{20}N_4Cl_4Mn$ 717.332; found 681.281.

$(FPh)_3CorMn^{IV}Cl$ 6. 13.9 mg, yield 91%. IR (KBr): ν, cm^{-1} 3100, 2921, 2853, 1596, 1504, 1412, 1355, 1301, 1228, 1154, 1030, 805, 723, 606, 524. UV-vis (CH_3CN): λ_{max}, nm (log ε) 313 (4.53), 358 (4.58), 431 (4.84). MS (MALDI-TOF): *m/z* calcd. for $C_{37}H_{20}N_4F_3ClMn$ 667.968; found 633.246.

$Ph_3CorMn^{IV}Cl$ 7. 13.4 mg, yield 90%. IR (KBr): ν, cm^{-1} 3051, 2925, 1602, 1507, 1427, 1351, 1301, 1158, 1058, 1027, 988, 845, 787, 757, 710, 664. UV-vis (CH_3CN): λ_{max}, nm (log ε) 312 (3.89), 357 (3.98), 430 (4.22). MS (MALDI-TOF): *m/z* calcd. for $C_{37}H_{23}N_4Mn$ 613.996; found 579.076.

$(CH_3Ph)_3CorMn^{IV}Cl$ 8. 18.4 mg, yield 92%. IR (KBr): ν, cm^{-1} 3112, 2925, 2860, 1729, 1560, 1513, 1452, 1371, 1295, 1175, 1120, 1059, 1026, 799, 723, 624. UV-vis (CH_3CN): λ_{max}, nm (log ε) 315 (4.21), 364 (4.29), 439 (4.47). MS (MALDI-TOF): *m/z* calcd. for $C_{40}H_{29}N_4ClMn$ 656.076; found 621.261.

RESULT AND DISCUSSION

Electrochemistry in CH_3CN and CH_2Cl_2

The investigated corroles undergo three types of redox processes in CH_3CN and CH_2Cl_2. One is a ring-centered oxidation involving conversion of a Mn^{IV} corrole to a Mn^{IV} π-cation radical and the other two involve metal-centered processes, Mn^{III}/Mn^{II} and either Mn^{III}/Mn^{IV} or Mn^{IV}/Mn^{III} depending upon the initial oxidation state of the central metal ion in **1–8**. Examples of cyclic voltammograms are shown in Fig. 1 for $(ClPh)_3CorMn^{III}$ **1** and $(ClPh)_3CorMn^{IV}Cl$ **5** and a summary of half-wave or peak potentials for each redox process of the eight compounds is given in Table 1 which compares the ring- and metal-centered redox processes for **1–4** and **5–8** as a function of the specific electron transfer process which occurs in each solvent, *i.e.* formation of a corrole π-cation radical or oxidation/reduction of the corrole central metal ion.

As seen in the table and figure, the Mn^{III}/Mn^{IV} reaction of **1–4** is characterized by two reversible redox processes in CH_3CN or CH_2Cl_2. The first occurs at $E_{1/2}$ values between 0.08 and 0.24 V and the second at $E_{1/2}$ = 0.31 to 0.45 V *vs.* SCE. Both oxidations are reversible and the current is smaller for the first process than for the second.

Similar redox behavior was previously reported for other manganese(III) triarylcorroles under similar solution conditions [10] and the "split" oxidation processes were assigned as resulting from two different Mn^{IV} corrole products, one which was ion-paired with the ClO_4^- from the supporting electrolyte, the other existing in its dissociated cationic form, *i.e.* $(YPh)_3CorMn^{IV}ClO_4$ and $[(YPh)_3CorMn^{IV}]^+$, respectively.

In contrast to the two Mn^{III}/Mn^{IV} oxidations in CH_3CN and CH_2Cl_2, only a single Mn^{IV}/Mn^{III} transition is exhibited for **5–8** in these two solvents (see Fig. 1b). The reversible $E_{1/2}$ values for the Mn^{IV}/Mn^{III} reductions of $(YPh)_3CorMnCl$ range from 0.07 to 0.23 V, values which are virtually identical to $E_{1/2}$ values for the first metal-centered oxidation of the neutral Mn(III) corroles in the same solvents. For example, $E_{1/2}$ = 0.24 V for oxidation of the *para*-chlorophenyl complex **1** in CH_3CN and 0.23 V for the reduction of the *para*-chlorophenyl complex **5** in the same solvent. Additional comparisons can be seen in Table 1 where in each case the $E_{1/2}$ values for reduction of Mn^{IV} in **5–8** are within experimental error of the measured potentials for the first Mn^{III} oxidation of **1–4**.

As will be demonstrated, the one-electron reduction of $(YPh)_3CorMn^{IV}Cl$ leads to a stable anionic Mn^{III} corrole with an axially coordinated chloride anion,

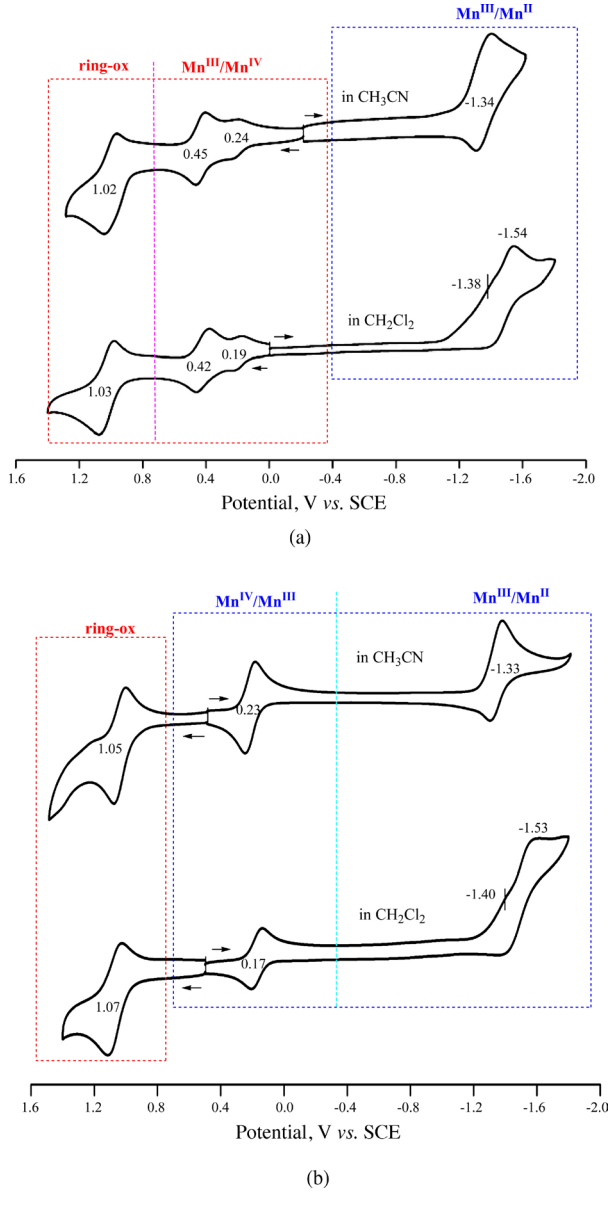

Fig. 1. Cyclic voltammograms of (a) $(ClPh)_3CorMn^{III}$ **1** and (b) $(ClPh)_3CorMn^{IV}Cl$ **5** in CH_3CN and CH_2Cl_2 containing 0.1 M TBAP. Scan rate = 0.10 V/s

i.e. $[(YPh)_3CorMn^{III}Cl]^-$, as opposed to $(YPh)_3CorMn^{III}$. However, the potentials for reduction of the five-coordinate Mn^{III} corroles electrogenerated from **5–8** are virtually identical to the $E_{1/2}$ values for reduction of the neutral four-coordinate Mn^{III} corroles **1–4** which lack an anionic ligand. These values are given in Fig. 1 and Table 1 where $E_{1/2}$ varies with the phenyl-ring substituent and ranges from -1.33 to -1.40 V in CH_3CN.

The similar potentials for reduction of the two compounds in each series (**1/5**, **2/6**, **3/7** and **4/8**) suggests that there is a fast dissociation of the Cl^- axial ligand on the electrogenerated $[(YPh)_3CorMn^{III}Cl]^-$ complexes prior to further electroreduction at -1.33 to -1.40 V in CH_3CN or CH_2Cl_2. This electrochemical *EC* mechanism is shown in Equation 1.

$$[(YPh)_3\,CorMn^{III}Cl]^- \underset{}{\overset{-Cl^-}{\rightleftharpoons}} (YPh)_3\,CorMn^{III} \overset{+e}{\rightleftharpoons} [(YPh)_3\,Mn^{II}]^- \quad (1)$$

A more complex situation is seen in CH_2Cl_2 for the Mn^{III}/Mn^{II} process which occurs in two steps as seen in Fig. 1. In brief, the first reduction of Mn^{III} at -1.38 to -1.47 V generates a Mn^{II} corrole which reacts with the solvent to give a second Mn^{III} corrole that is then irreversibly reduced to Mn^{II} at a peak potential of -1.53 to -1.72 V (see E_p values in Table 1). This mechanism has been examined in detail for related Mn^{III} octaethylcorroles and is described in the literature [9]. It is not a subject of the current publication since the same chemical reactions occur for **1–4** and **5–8** and these are not related to the initial oxidation state of the corrole central metal ion.

In summary, the two metal-centered electrode reactions of $(YPh)_3CorMn^{III}$ and $(YPh)_3CorMn^{IV}Cl$ in CH_3CN and CH_2Cl_2 are proposed to occur as shown in Scheme 1 where only the first of two $Mn^{III/II}$ processes is illustrated.

Electrochemistry in pyridine

Mn^{III} corroles have been shown to axially coordinate one pyridine [10, 11, 26] and this is also the case for the currently examined Mn^{III} corroles **1–4** which exist as five-coordinate complexes in pyridine containing 0.1 M TBAP. Cyclic voltammograms of $(YPh)_3CorMn^{III}(py)$ **1–4** under these solution conditions are shown in Fig. 2a. Each corrole undergoes a well-defined reversible reduction at -1.30 to -1.37 V and a more complicated $Mn^{III/IV}$ oxidation which involves non-coupled oxidation/reduction peaks as seen in the figure.

The mechanism for oxidation of related Mn^{III} corroles in pyridine has been described in a previous publication as involving an electrochemical "box scheme" [10] and the same sequence of steps is proposed to occur for oxidation of the five-coordinate $(YPh)_3CorMn(py)$ derivatives **1–4** in this solvent. This prevailing mechanism is given in the top part of Scheme 2 where $(YPh)_3CorMn^{III}(py)$ **1–4** (shown in blue and bold) is initially oxidized to $[(YPh)_3CorMn^{IV}(py)]^+$ at $E_{1/2} = 0.45$–0.53 V. This electrochemical reaction is then followed by rapid addition of a second pyridine molecule to give $[(YPh)_3CorMn^{IV}(py)_2]^+$ which is re-reduced at 0.30–0.38 V on the reverse scan to give a transient six-coordinate $(YPh)_3CorMn^{III}(py)_2$, after which one pyridine dissociates to give back the original five-coordinate complex. The main Mn^{IV} species in solution after oxidation of $[(YPh)_3CorMn^{IV}(py)]^+$ is $[(YPh)_3CorMn^{IV}(py)_2]^+$ but because the oxidized five-coordinate complex is easier to re-reduce than the oxidized bis-pyridine derivative, a dissociation of one bound py ligand occurs prior to electron transfer (an electrochemical *CE* mechanism)

Table 1. Half-wave potentials (V *vs.* SCE) for redox reactions of $(YPh)_3CorMn^{III}$ **1–4** and $(YPh)_3CorMn^{IV}Cl$ **5–8** in CH_2Cl_2, CH_3CN and pyridine containing 0.1 M TBAP

Solvent	Compound	Corrole ring ox		Metal rxn		Metal red, $Mn^{III/II}$[a]	
		cpd **1–4**	cpd **5–8**	Mn^{IV} red (**5–8**)	Mn^{III} ox (**1–4**)	cpd **1–4**	cpd **5–8**
CH_3CN	Y = Cl **1, 5**	1.02	1.05	0.23	0.24, 0.45	-1.34	-1.33
	Y = F **2, 6**	0.99	1.03	0.21	0.23, 0.42	-1.36	-1.36
	Y = H **3, 7**	0.96	1.02	0.18	0.21, 0.39	-1.38	-1.38
	Y = CH_3 **4, 8**	0.92	0.97	0.14	0.18, 0.35	-1.39	-1.40
CH_2Cl_2	Y = Cl **1, 5**	1.03	1.07	0.17	0.19, 0.42	-1.38[b] (-1.54[b])[d]	-1.40[b] (-1.53[b])[d]
	Y = F **2, 6**	1.02	1.05	0.14	0.16, 0.39	-1.40[b] (-1.66[b])[d]	-1.42[b] (-1.66[b])[d]
	Y = H **3, 7**	0.99	1.03	0.09	0.12, 0.32	-1.46[b] (-1.70[b])[d]	-1.44[b] (-1.70[b])[d]
	Y = CH_3 **4, 8**	0.94	0.97	0.07	0.08, 0.31	-1.47[b] (-1.72[b])[d]	-1.46[b] (-1.72[b])[d]
Pyridine	Y = Cl **1, 5**			0.49[b,c], 0.32[b]	0.38, 0.53	-1.30	-1.31
	Y = F **2, 6**			0.49[b,c], 0.25[b]	0.37, 0.52	-1.33	-1.32
	Y = H **3, 7**			0.46[b,c], 0.22[b]	0.33, 0.49	-1.34	-1.34
	Y = CH_3 **4, 8**			0.42[b,c], 0.22[b]	0.30, 0.45	-1.37	-1.37

[a] The Mn^{III} reduction is assigned as metal-centered in CH_3CN and CH_2Cl_2 and ring-centered in pyridine; see discussion in text. [b] Irreversible peak potential at a scan rate of 0.10 V/s. [c] Re-oxidation peak potential at a scan rate of 0.1 V/s. [d] The second reduction in parentheses involves product of the Mn^{II} chemical reaction.

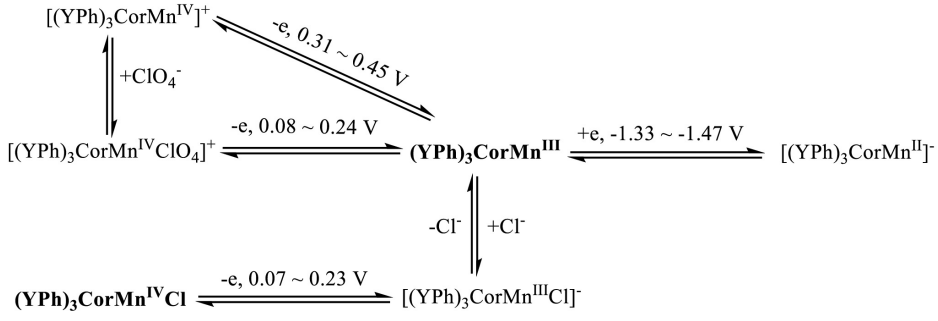

Scheme 1. Proposed redox mechanism for the metal-centered reactions of $(YPh)_3CorMn^{III}$ and $(YPh)_3CorMn^{IV}Cl$ in CH_3CN and CH_2Cl_2 containing 0.1 M TBAP

and both $Mn^{IV/III}$ re-reductions are detected on the cyclic voltammetry timescale, one at $E_{1/2}$ = 0.45–0.53 V and the other at E_p = 0.30–0.38 V for a scan rate of 0.10 V/s.

A similar "box mechanism" also occurs for conversion of $(YPh)_3CorMn^{IV}Cl$ **5–8** to its Mn^{III} form (Scheme 2, bottom). The chloride bound compound in solution is irreversibly reduced at a peak potential of 0.22–0.32 V in pyridine to give $[(YPh)_3CorMn^{III}Cl]^-$ as seen in Fig. 2b. This anionic product is not stable in pyridine and undergoes a replacement of bound Cl^- for a py molecule, leading to the formation of neutral $(YPh)_3CorMn^{III}(py)$ which is re-oxidized at 0.42–0.49 V to reform the initial compound after a Cl^- for py exchange of axial ligand as shown in Scheme 2. The opposite ligand exchange reaction, a conversion of $(YPh)_3CorMn^{IV}Cl$ to $[(YPh)_3CorMn^{IV}(py)]^+$, does not occur, even in neat pyridine, and the UV-visible spectrum of neutral $(YPh)_3CorMn^{IV}Cl$ in pyridine is the same as in CH_2Cl_2 or CH_3CN (see later discussion).

The reduction of Mn^{III} corroles **1–4** in pyridine is assigned to a corrole ring-centered reaction to generate a Mn^{III} π-anion radical and no $Mn^{III/II}$ process is observed in this solvent. Almost exactly the same potential is seen for the second reduction of the structurally similar Mn^{IV} corroles **5–8** (Fig. 2b) as for the first reduction of compounds **1–4** (see Fig. 2a). For example, the reversible potential for the first reduction of $(CH_3Ph)_3CorMn^{III}$ **4** is located at $E_{1/2}$ = -1.37 V and the same half-wave potential is seen for the second reduction of $(CH_3Ph)_3CorMn^{IV}Cl$ **8**. Therefore, it is reasonable to conclude that the electron transfer mechanism for the second one-electron reduction of the Mn^{IV} corroles **5–8** is the same as that for the first one-electron reduction of the Mn^{III} corroles **1–4**, namely, formation of a Mn^{III} corrole π-anion radical.

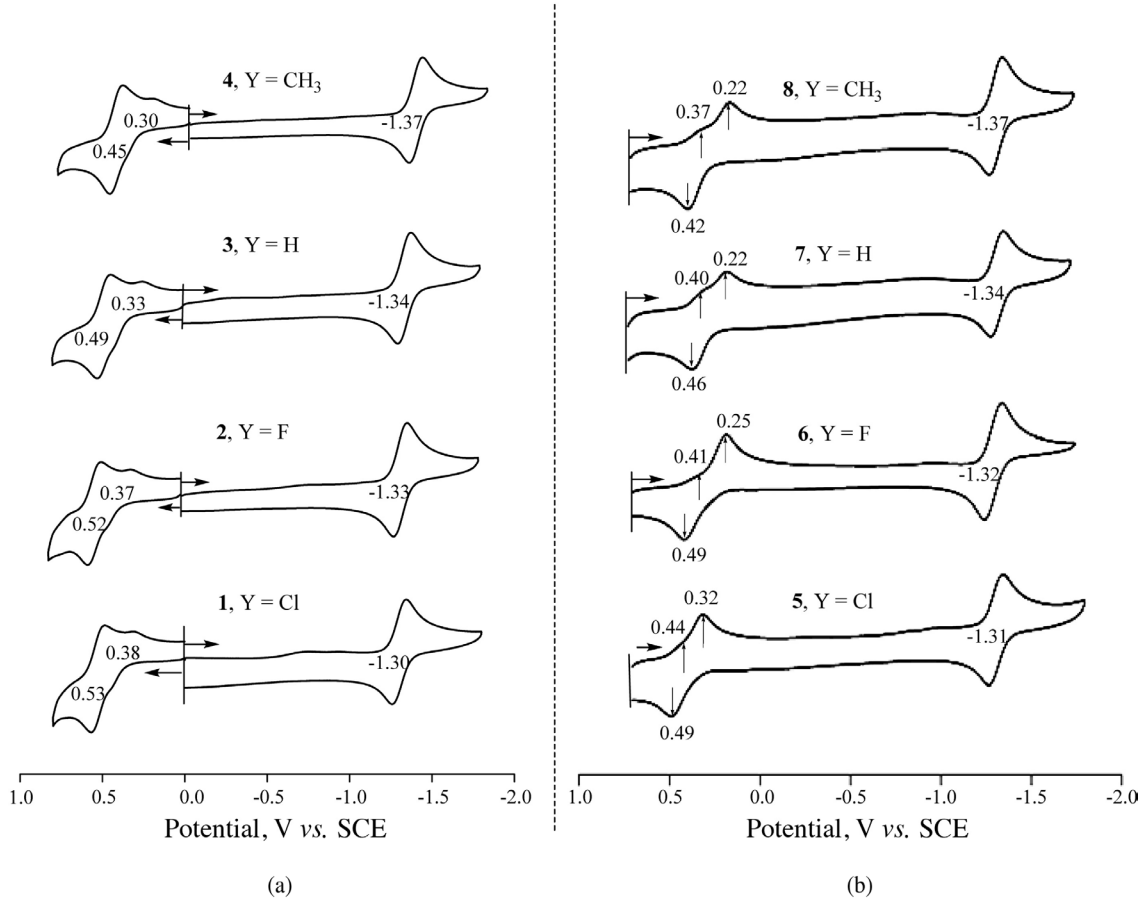

Fig. 2. Cyclic voltammograms of (a) $(YPh)_3CorMn^{III}$ **1–4** and (b) $(YPh)_3CorMn^{IV}Cl$ **5–8** in pyridine containing 0.1 M TBAP. Scan rate = 0.10 V/s

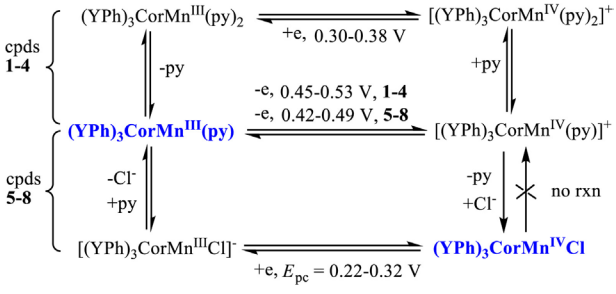

Scheme 2. Proposed "box mechanism" for redox reactions of Mn^{III} corroles **1–4** and Mn^{IV} corroles **5–8** in pyridine containing 0.1 M TBAP. The initial compounds are shown in bold blue color

Effect of substituents on redox potentials

The effect of substituents on redox potentials for a given set of structurally related porphyrins or corroles with different electron-donating or electron-withdrawing substituents can often be quantitated by the linear free energy relationship $E_{1/2} = \Sigma\sigma\rho$ [27–29], where $E_{1/2}$ is the half-wave potential for each redox process of the compound, σ is the Hammett substituent constant and ρ, measured in volt, represents the sensitivity of the given redox reaction to the change of substituent. In the case of *para*-substituted tetraphenylporphrins (TPP) the value of ρ generally ranges from 50 to 100 mV, depending upon solvent, the central metal ion and the site of electron transfer [30]. The larger the value of ρ, the greater is the effect of the substituent on the specific redox reaction. In general, oxidations or reductions at the porphyrin π-ring system will be more sensitive to *para*-phenyl substituents than metal-centered reactions and this fact has sometimes been used to assign the site of electron transfer [27, 30].

Triaryl-substituted corroles have been shown to have similar substituent effects as tetraaryl-substituted porphyrins [10, 31, 32], with the relevant linear free energy equation being $\Delta E_{1/2} = 4\sigma\rho$ in the case of porphyrins with four *meso* substituted-phenyl groups and $\Delta E_{1/2} = 3\sigma\rho$ in the case of corroles with three *meso* substituted-phenyl groups. Figure 3 illustrates examples of these plots for $(YPh)_3CorMn^{III}$ **1–4** and $(YPh)_3CorMn^{IV}Cl$ **5–8** in CH_3CN and pyridine. Linear relationships are observed between $E_{1/2}$ and 3σ for each electrode reaction, with the slope (ρ) of the straight line ranging from 43 to 85 mV. In pyridine the oxidation and reduction have similar ρ values which are little affected by the initial metal

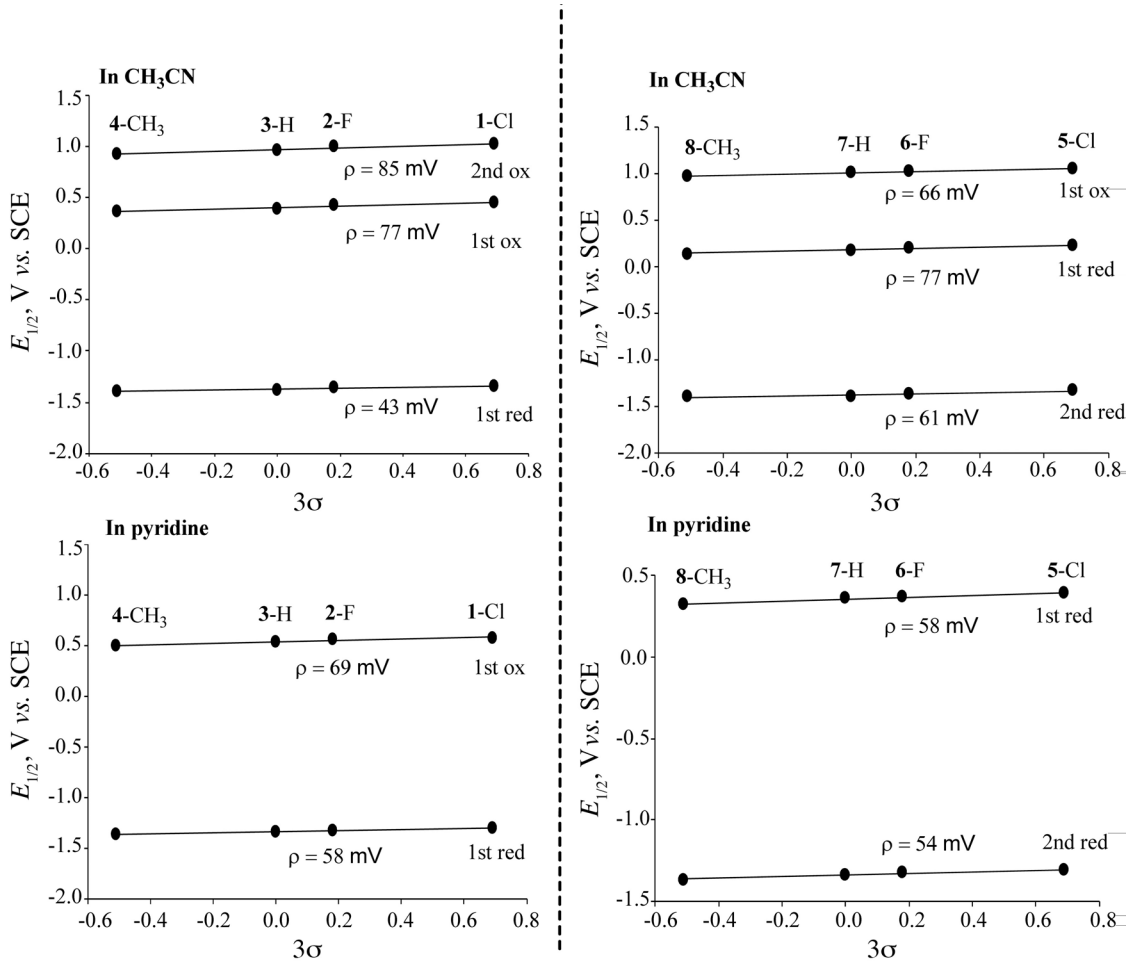

(a) Mn^{III} Corroles **1-4** (b) Mn^{IV} Corroles **5-8**

Fig. 3. Substituent effects on half-wave potentials in different solvents. Plots of measured potentials for oxidation and reduction of **1–4** and **5–8** *vs*. the sum of the Hammett substituent constants 3σ. Values of σ taken from reference 28

oxidation state on the compound or the site of electron transfer (π-ring system upon reduction and central metal ion upon oxidation). A more significant difference is seen in CH_3CN where ρ for the Mn^{III}/Mn^{II} reaction is smaller than for the metal- and ring-centered oxidations. There are no unexpected trends in the data of Fig. 3 and linear free energy relationships are observed for all of the compounds in the two series of corroles.

UV-visible spectra of neutral corroles 1–8

UV-visible spectra of $(YPh)_3CorMn^{III}$ **1–4** and $(YPh)_3CorMn^{IV}Cl$ **5–8** were measured in CH_3CN, CH_2Cl_2 and pyridine prior to oxidation and reduction. Examples of the spectra for $(FPh)_3CorMn^{III}$ **2** and $(FPh)_3CorMn^{IV}Cl$ **6** in the three solvents containing 0.1 M TBAP are illustrated in Fig. 4.

$(FPh)_3CorMn^{III}$ **2** has the same UV-visible spectrum in CH_2Cl_2 and CH_3CN but a different spectrum is exhibited in pyridine due to formation of the five-coordinate $(FPh)_3CorMn^{III}(py)$ in this solvent. These spectra are shown in Fig. 4a and are consistent with what was earlier reported for other Mn^{III} triarylcorroles which easily bind one pyridine molecule under the same solution conditions [10, 26].

The chloride bound Mn^{IV} corroles **5–8** do not bind pyridine as demonstrated for $(FPh)_3CorMn^{IV}Cl$ **6** where an identical spectrum is observed in all three solvents (Fig. 4b). As can be seen in this figure, the electronic absorption spectrum of $(FPh)_3CorMn^{IV}Cl$ **6** is quite different from that of $(FPh)_3CorMn^{III}$ in CH_3CN or CH_2Cl_2 or $(FPh)_3CorMn^{III}(py)$ in pyridine, consistent with two different oxidation states of the manganese central ion.

UV-visible spectra of oxidized and reduced corroles

Compounds **1–8** were examined by thin-layer UV-visible spectroelectrochemistry during controlled potential oxidation or reduction and examples of the spectral changes obtained for $(ClPh)_3CorMn^{III}$ **1** and $(ClPh)_3CorMn^{IV}Cl$ **5** in CH_2Cl_2 are shown in Fig. 5.

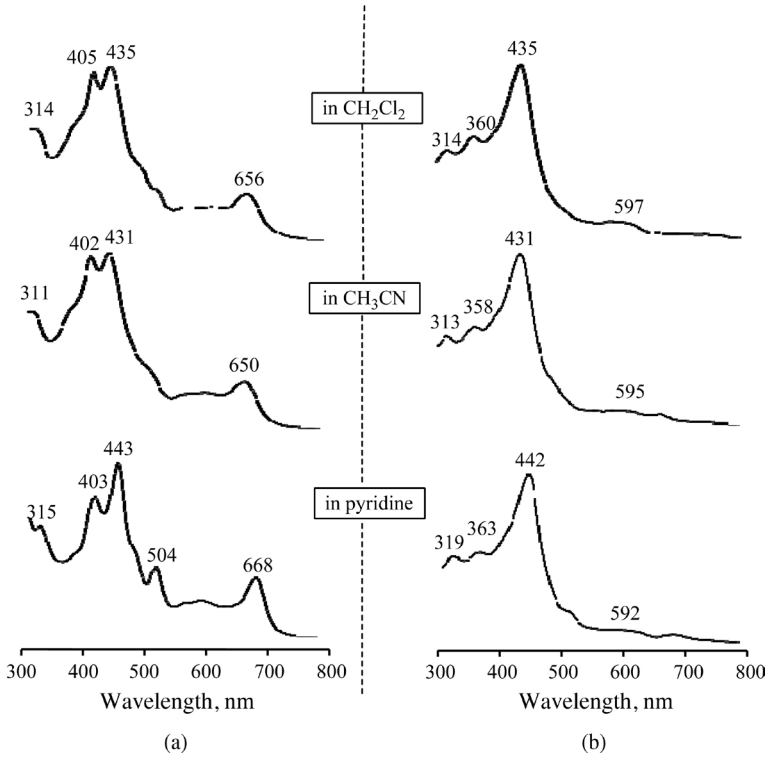

Fig. 4. UV-visible spectra of neutral (a) $(FPh)_3CorMn^{III}$ **2** and (b) $(FPh)_3CorMn^{IV}Cl$ **6** in CH_2Cl_2, CH_3CN and pyridine containing 0.1 M TBAP

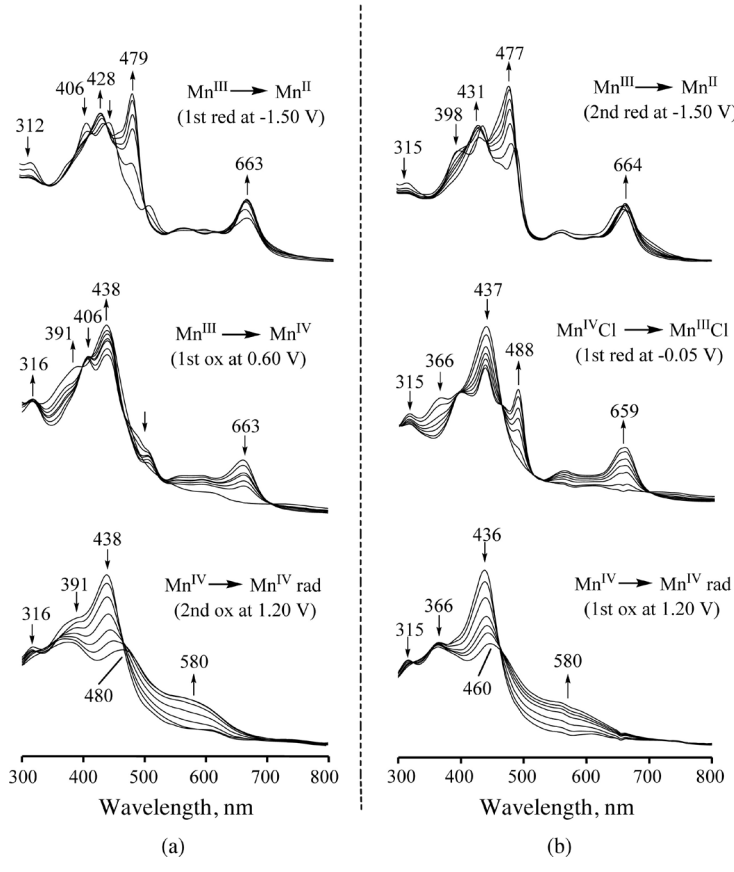

Fig. 5. Thin-layer UV-visible spectral changes of (a) $(ClPh)_3CorMn^{III}$ **1** and (b) $(ClPh)_3CorMn^{IV}Cl$ **5** during the controlled potential reduction and oxidation in CH_2Cl_2 containing 0.1 M TBAP

The spectrum obtained after reduction of **1** in the thin-layer cell at a controlled potential of -1.50 V has bands at 428, 479, and 663 nm (top spectra in Fig. 5a), and the product is assigned as a Mn^{II} corrole rather than a corrole π-anion radical. Similar spectral changes result during the first reduction of compounds **2–4** in CH_2Cl_2 and CH_3CN as well as during the second reduction of **5** (top spectra in Fig. 5b). These results are consistent with a Mn^{III}/Mn^{II} transition in each case [9–11].

The first oxidation of structurally related Mn^{III} corroles has been described as a metal-centered reaction to generate a Mn^{IV} corrole [2, 9–12, 33, 34] and this is what is observed for $(ClPh)_3CorMn^{III}$ **1** after the abstraction of one electron in CH_2Cl_2 at a controlled potential of 0.60 V (see middle spectra in Fig. 5a). Further oxidation of the Mn^{IV} corrole at 1.20 V (bottom spectra of Fig. 5a) leads to an intensity decreased Soret band and the appearance of new bands at 480 and ~580 nm. The final spectrum is assigned as a Mn^{IV} corrole π-cation radical, consistent with earlier assignments in the literature [9–11, 35–37]. The same types of spectral changes are observed for the second oxidation of compounds **2**, **3** and **4** in CH_2Cl_2 and for the first oxidation of **5** under the same solution conditions (Fig. 5b, bottom).

It should be pointed out that the final spectrum of the Mn^{III} product obtained after the first reduction of compound **5** differs from that of the Mn^{III} neutral compound **1** (two middle spectra in Figs 5a and 5b). The product electrochemically generated at -0.05 V from **5** is assigned as a Mn^{III} corrole with a bound chloride ion, *i.e.* $[(ClPh)_3CorMn^{III}Cl]^-$. This five-coordinate species could also be generated in solution by a titration of TBACl into a CH_3CN solution of neutral $(ClPh)_3CorMn^{III}$. The final chloride bound Mn^{III} species has bands at 398, 432, 483 and 650 nm as seen

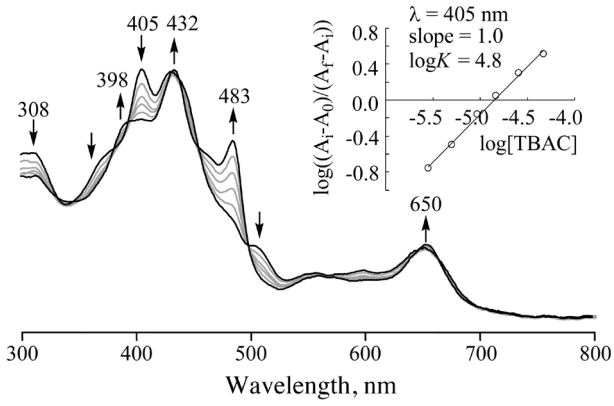

Fig. 6. UV-visible spectral changes during titration of $(ClPh)_3CorMn^{III}$ **1** with TBACl in CH_3CN. The insert shows the diagnostic log-log plot for analyzing the number of bound chloride ions and the formation constant

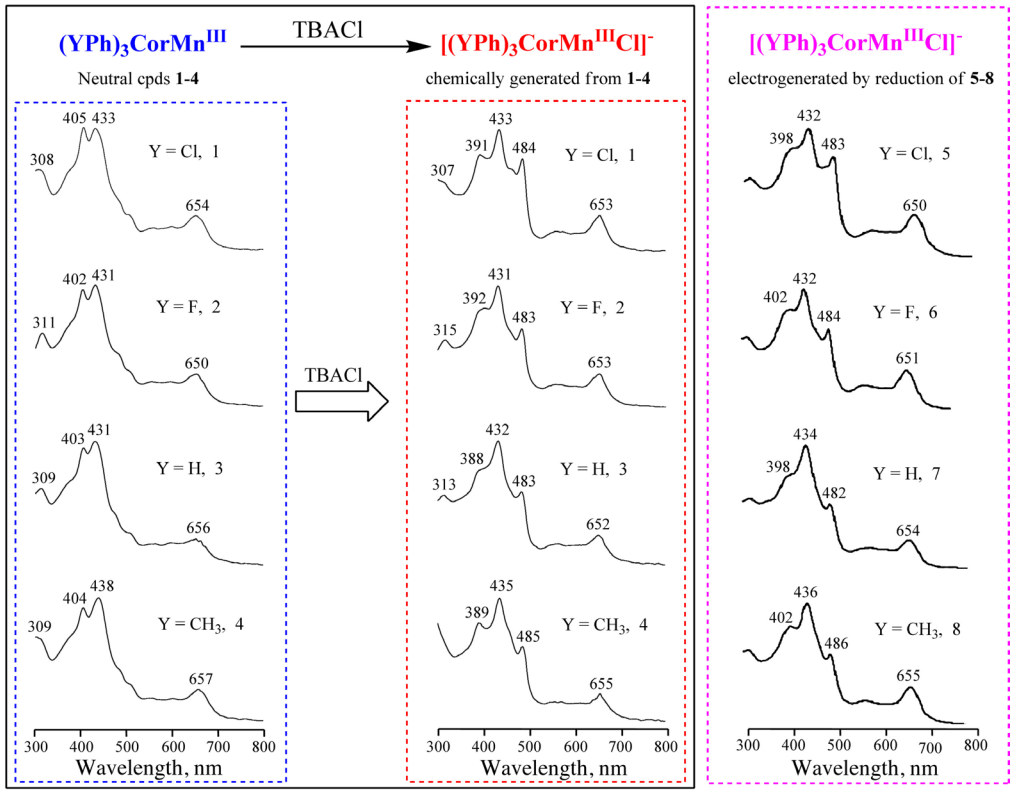

Fig. 7. UV-visible spectra of neutral $(YPh)_3CorMn^{III}$ **1–4** in CH_3CN, the $[(YPh)_3CorMn^{III}Cl]^-$ generated after addition of TBACl into the solution of compounds **1–4** in CH_3CN and the $[(YPh)_3CorMn^{III}Cl]^-$ electrogenerated after the first controlled potential reduction of compounds **5–8** in CH_3CN containing 0.1 M TBAP

Table 2. Comparison of the UV-vis spectral data (λ_{max}, nm) between electrogenerated and chemically synthesized Mn^{IV} corroles, $[(YPh)_3CorMn^{IV}]^+$, in CH_2Cl_2, CH_3CN and pyridine containing 0.1 M TBAP

Solvent	Compound	Electrogenerated $(YPh)_3CorMn^{IV}ClO_4$	Compound	Synthesized $(YPh)_3CorMn^{IV}Cl$
CH_2Cl_2	**1,** Y = Cl	316, 391, 438, 612	**5,** Y = Cl	315, 366, 437, 601
	2, Y = F	318, 383, 435, 609	**6,** Y = F	314, 360, 435, 602
	3, Y = H	313, 362, 434, 606	**7,** Y = H	312, 358, 434, 600
	4, Y = CH_3	320, 387, 444, 600	**8,** Y = CH_3	318, 361, 441, 601
CH_3CN	**1,** Y = Cl	312, 361, 433, 598	**5,** Y = Cl	313, 363, 431, 596
	2, Y = F	311, 370, 429, 601	**6,** Y = F	313, 358, 431, 595
	3, Y = H	312, 362, 429, 610	**7,** Y = H	312, 357, 430, 600
	4, Y = CH_3	317, 363, 439, 620	**8,** Y = CH_3	315, 364, 439, 625
Pyridine[a]	**1,** Y = Cl	320, 402, 443, 505, 677	**5,** Y = Cl	318, 365, 443, 600
	2, Y = F	315, 402, 441, 504, 672	**6,** Y = F	319, 363, 442, 592
	3, Y = H	318, 405, 442, 501, 681	**7,** Y = H	317, 362, 439, 670
	4, Y = CH_3	316, 397, 441, 507, 689	**8,** Y = CH_3	320, 361, 445, 665

[a]The singly oxidized species from the Mn^{III} corroles **1–4** is assigned to the $(YPh)_3CorMn^{IV}(py)_2$ in pyridine, see discussion in text.

Table 3. Comparison of the UV-vis spectral data (λ_{max}, nm) between the chemically synthesized and electrogenerated Mn^{III} corroles in CH_2Cl_2, CH_3CN and pyridine containing 0.1 M TBAP

Solvent	Compound	Synthesized $(YPh)_3CorMn^{III}$	Compound	Electrogenerated $[(YPh)_3CorMn^{III}Cl]^-$
CH_2Cl_2	**1,** Y = Cl	312, 406, 436, 663	**5,** Y = Cl	398, 436, 488, 659
	2, Y = F	314, 405, 435, 656	**6,** Y = F	395, 435, 488, 656
	3, Y = H	312, 407, 433, 659	**7,** Y = H	391, 435, 484, 656
	4, Y = CH_3	308, 406, 445, 668	**8,** Y = CH_3	395, 438, 488, 656
CH_3CN	**1,** Y = Cl	308, 405, 433, 654	**5,** Y = Cl	398, 432, 483, 650
	2, Y = F	311, 402, 431, 650	**6,** Y = F	402, 432, 484, 651
	3, Y = H	309, 403, 431, 656	**7,** Y = H	398, 434, 482, 654
	4, Y = CH_3	309, 404, 438, 657	**8,** Y = CH_3	402, 436, 486, 655
Pyridine[a]	**1,** Y = Cl	317, 405, 445, 505, 669	**5,** Y = Cl	318, 406, 444, 504, 671
	2, Y = F	315, 403, 443, 504, 668	**6,** Y = F	319, 405, 443, 504, 669
	3, Y = H	317, 405, 444, 505, 670	**7,** Y = H	317, 400, 440, 501, 668
	4, Y = CH_3	316, 404, 445, 506, 673	**8,** Y = CH_3	320, 405, 445, 508, 674

[a]The neutral compounds **1–4** and the singly reduced species of the compounds **5–8** are assigned as Mn^{III}(py) in pyridine.

in Fig. 6 which includes a diagnostic plot of $\log((A_i - A_0)/(A_f - A_i))$ *vs.* log[TBACl]. The slope of the plot is 1.0 and the calculated binding constant is log$K$ = 4.8 for the reaction given in Equation 2.

$$(ClPh)_3CorMn^{III} + Cl^- \rightleftharpoons [(ClPh)_3CorMn^{III}Cl]^- \quad (2)$$

A comparison of UV-visible spectra for the chemically generated Mn^{III} corroles **1–4** in CH_3CN with a bound chloride ion with spectra of the electrogenerated $[(YPh)_3CorMn^{III}Cl]^-$ species from **5–8** is given in Fig. 7. As seen in this figure, the spectra of the singly reduced Mn^{IV} corroles are identical to spectra for the structurally related Mn^{III} corroles with added TBACl and both of

Table 4. Comparison of the UV-vis spectral data (λ_{max}, nm) of the singly reduced species from Mn^{III} corroles **1–4** and the doubly reduced species from Mn^{IV} corroles **5–8** in CH_2Cl_2, CH_3CN and pyridine containing 0.1 M TBAP

Solvent	Compound	Singly reduced $(YPh)_3CorMn^{II}$	Compound	Doubly reduced $(YPh)_3CorMn^{II}$
CH_2Cl_2	**1,** Y = Cl	428, 479, 663	**5,** Y = Cl	431, 477, 664
	2, Y = F	425, 478, 659	**6,** Y = F	426, 477, 661
	3, Y = H	426, 479, 662	**7,** Y = H	428, 479, 662
	4, Y = CH_3	420, 480, 654	**8,** Y = CH_3	424, 481, 659
CH_3CN	**1,** Y = Cl	428, 476, 660	**5,** Y = Cl	426, 476, 662
	2, Y = F	426, 473, 655	**6,** Y = F	421, 475, 657
	3, Y = H	424, 476, 660	**7,** Y = H	420, 476, 659
	4, Y = CH_3	424, 478, 661	**8,** Y = CH_3	423, 477, 661
Pyridine[a]	**1,** Y = Cl	317, 400, 433[b], 667	**5,** Y = Cl	398, 434[b], 671
	2, Y = F	315, 400, 430, 665	**6,** Y = F	318, 400, 430, 670
	3, Y = H	318, 402, 432, 663	**7,** Y = H	319, 398, 430, 669
	4, Y = CH_3	316, 403, 435, 675	**8,** Y = CH_3	319, 404, 434, 676

[a]The products are assigned to the Mn^{III} π-anion radicals in pyridine. [b]A peak at 481 nm can also be observed.

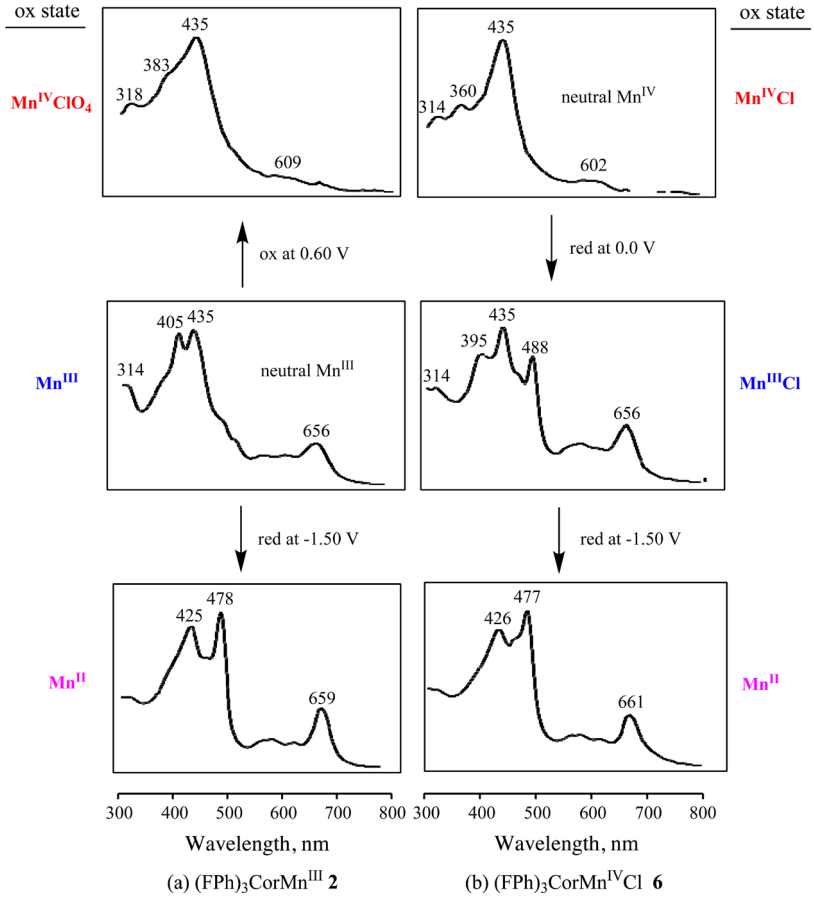

Fig. 8. UV-vis spectra of $(FPh)_3CorMn$ **2** and $(FPh)_3CorMnCl$ **6** in CH_2Cl_2 containing 0.1 M TBAP in their Mn^{IV}, Mn^{III} and Mn^{II} oxidation states

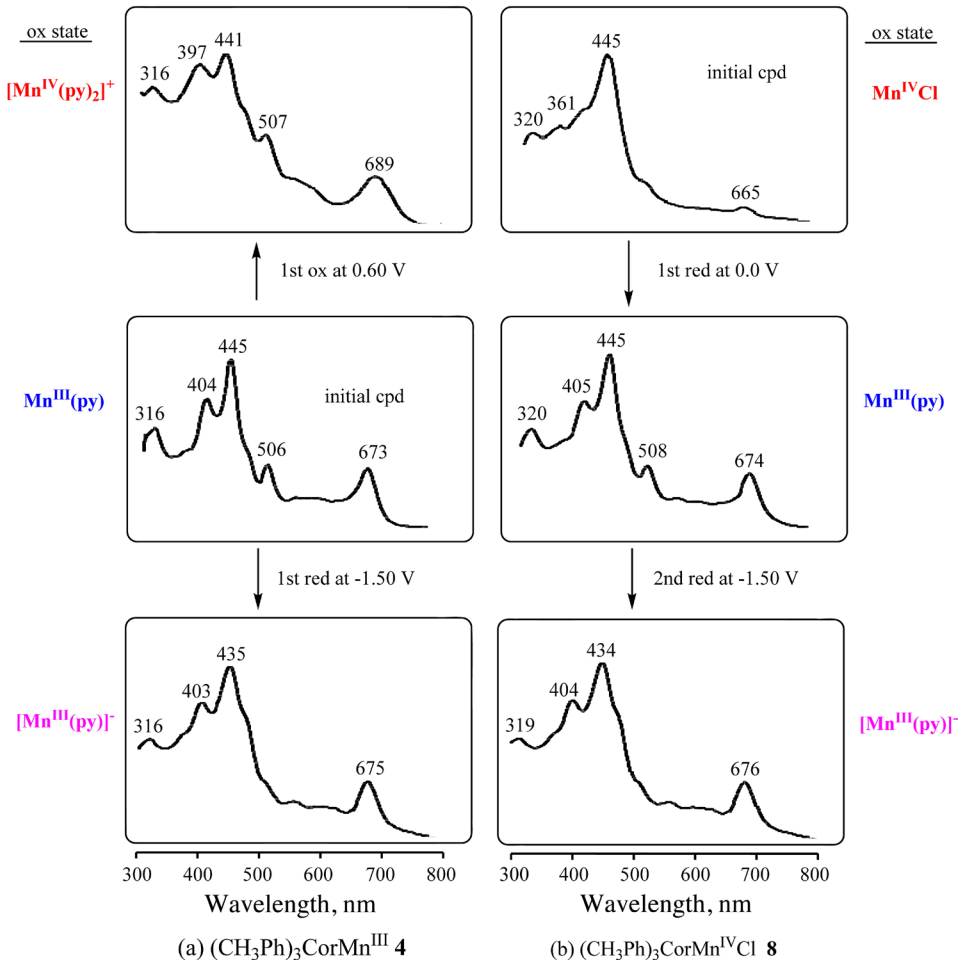

Fig. 9. UV-vis spectra of $(CH_3Ph)_3CorMn$ **4** and $(CH_3Ph)_3Cor\ MnCl$ **8** in pyridine containing 0.1 M TBAP in their different oxidation states of the central metal ion with different coordinated axial ligand

these spectra are different from the spectrum of the initial four-coordinate Mn^{III} complex.

Comparisons in spectra between the Mn^{IV}, Mn^{III} and Mn^{II} oxidation states of 1–4 and 5–8

A summary of the spectral data for the Mn^{IV}, Mn^{III} and Mn^{II} corroles is given in Tables 2–4 and a comparison of spectra for selected compounds in each metal oxidation state of the $(YPh)_3CorMn^{III}$ **1–4** and $(YPh)_3CorMn^{IV}Cl$ **5–8** is illustrated in Figs 8 and 9. Figure 8 compares spectra for compounds **2** and **6** in CH_2Cl_2 while a similar comparison is given in Fig. 9 for compounds **4** and **8** in pyridine. The last reduction of **1–8** in CH_2Cl_2 or CH_3CN corresponds to a Mn^{III}/Mn^{II} process while the last reduction of **1–8** in pyridine corresponds to the conversion of a Mn^{III} corrole to a Mn^{III} corrole π-anion radical as discussed in earlier sections of the manuscript. The same spectral patterns were obtained in CH_3CN and CH_2Cl_2 for each compound in a given oxidation state.

The spectral data in Tables 2–4 and in Figs 8 and 9 can be summarized as follows: in CH_3CN and CH_2Cl_2, virtually identical spectra are seen for: (a) the Mn^{IV} forms of **1–4** and **5–8** (top spectra in Fig. 8) and (b) the Mn^{II} forms of **1–4** and **5–8** (bottom spectra in Fig. 8). This is contrast with the Mn^{III} forms of **1–4** and **5–8** which are different in CH_3CN and CH_2Cl_2 due to different coordination numbers of the Mn^{III} compounds in the two series (see middle spectra in Fig. 8).

In pyridine, identical UV-visible spectra are seen for: (a) the Mn^{III} forms of **1–4** and **5–8** and (b) the Mn^{III} π-anion radical forms of **1–4** and **5–8**. This contrasts with the Mn^{IV} forms of the compounds in the two series which differ from each other as seen in the top two spectra of Fig. 9 for compounds **4** and **8**. This difference in UV-visible spectra is due to the different axial coordination of the Mn^{IV} corrole in the two series, Cl^- in the case of **5–8** and two pyridine molecules in the case of **1–4**. The exact spectral wavelengths of each compound in the four different oxidation states are given in the tables.

In summary, two related series of manganese substituted *meso*-triarylcorroles containing electron-withdrawing or electron-donating substituents on the macrocycle were examined as to their electrochemistry

and spectroelectrochemistry in CH_2Cl_2, CH_3CN and pyridine. One series consisted of neutral four-coordinate Mn^{III} complexes and the other was comprised five-coordinate Mn^{IV} corroles with a chloride axial ligand. The effect of solvent, coordination number and metal oxidation state on the UV-visible spectra and redox potentials of each compound were examined in the three solvents and a mechanism for each oxidation/reduction process was proposed after analysis of the redox potentials and the spectroelectrochemical data. The use of spectroelectrochemistry is the key to identify the electroactive species and the products of each redox reaction which could not be done by electrochemical measurements alone.

Acknowledgements

This work was supported by the Natural Science Foundation of China (Grant No. 21071067) and the Robert A. Welch Foundation (KMK, E-680).

Supporting information

Supplementary materials are available free of charge *via* the Internet at http://www.worldscinet.com/jpp/jpp.shtml.

REFERENCES

1. Paolesse R. In *The Porphyrin Handbook*, Vol. 2, Kadish KM, Smith KM and Guilard R. (Eds.) Academic Press: San Diego, 2000; pp 201–232.
2. Erben C, Will S and Kadish KM. In *The Porphyrin Handbook*, Vol. 2, Kadish KM, Smith KM and Guilard R. (Eds.) Academic Press: San Diego, 2000; pp 233–300.
3. Gross Z and Gray HB. *Comm. Inorg. Chem.* 2006; **27**: 61–72.
4. Aviv I and Gross Z. *Chem. Commun*. 2007; **20**: 1987–1999.
5. Aviv-Harel I and Gross Z. *Chem. Eur. J.* 2009; **15**: 8382–8394.
6. Guilard R, Barbe JM, Stern C and Kadish KM. In *The Porphyrin Handbook,* Vol. 18, Kadish KM, Smith KM and Guilard R. (Eds.) Academic Press: New York, 2003; pp 303–349.
7. McGown AJ, Badiei YM, Leeladee P, Prokop KA, DeBeer S and Goldberg DP. In *Handbook of Porphyrin Science,* Vol. 14, Kadish KM, Smith KM and Guilard R. (Eds.) Academic Press: New York, 2011; pp 525–599.
8. Liu HY, Mahmood MH, Qiu SX and Chang CK. *Coord. Chem. Rev.* 2013; **257**: 1306–1333.
9. Ou ZP, Erben C, Autret M, Will S, Rosen D, Lex J, Vogel E and Kadish KM. *J. Porphyrins Phthalocyanines* 2005; **9**: 398–412.
10. Shen J, Ojaimi ME, Chkounda M, Gros CP, Barbe JM, Shao J, Guilard R and Kadish KM. *Inorg. Chem*. 2008; **47**: 7717–7727.
11. Chen P, Ojaimi ME, Gros CP, Barbe J-M, Guilard R, Shen J and Kadish KM. *J. Porphyrins Phthalocyanines* 2011; **15**: 188–196.
12. Golubkov G, Bendix J, Gray HB, Mahammed A, Goldberg I, DiBilio AJ and Gross Z. *Angew. Chem. Int. Ed.* 2001; **40**: 2132–2134.
13. Liu HY, Lai TS, Yeung LL and Chang CK. *Org. Lett.* 2003; **5**: 617–620.
14. Collman JP, Kaplun M and Decreau RA. *Dalton Trans*. 2006; 554–559.
15. Ye LN, Ou ZP, Meng DY, Yuan MZ, Fang YY and Kadish KM. *J. Turkish Chem.* 2014; **38**: 994–1005.
16. Gross Z, Golubkov G and Simkhovich L. *Angew. Chem. Int. Ed*. 2000; **39**: 4045–4047.
17. Gross Z and Gray HB. *Adv. Synth. Catal*. 2004; **346**: 165–170.
18. Lvova L, Di Natale C, D'Amico A and Paolesse R. *J. Porphyrins Phthalocyanines* 2009; **13**: 1168–1178.
19. Ding M, Wang B, Wang Z, Zhang J, Fuhr O, Fenske D and Gao S. *Chem. Eur. J*. 2012; **18**: 915–924.
20. Okun Z, Kupershmidt L, Youdim MBH and Gross Z. *Anticancer Agents Med. Chem*. 2011; **11**: 380–384.
21. Lim P, Mahammed A, Okun Z, Saltsman I, Gross Z, Gray HB and Termini J. *Chem. Res. Toxicol.* 2012; **25**: 400–409.
22. Xia M, Liu JH, Gao Y, Akermark B and Sun LC. *Helvetica Chim. Acta* 2007; **90**: 553–561.
23. Lei HT, Han A. Li FW; Zhang MN, Han YZ, Du PW, Lai WZ and Cao R. *Phys. Chem. Chem. Phys*. 2014; **16**: 1883–1893.
24. Steene E, Wondimagegn TW and Ghosh A. *J. Phys. Chem*. B 2001; **105**: 11406–11413.
25. Koszarna B and Gryko DT. *J. Org. Chem*. 2006; **71**: 3707–3717.
26. Licoccia S, Morgante E, Paolesse R, Polizio F, Senge MO, Tondello E and Boschi T. *Inorg. Chem*. 1997; **36**: 1564–1570.
27. Kadish KM, Van Camelbecke E and Royal G. In *The Porphyrin Handbook*, Vol. 8, Kadish KM, Smith KM and Guilard R. (Eds.) Academic Press: New York, 2000; Chapter 55, pp 1–114.
28. Zuman P. *Substituent Effects in Organic Polarography,* Plenum Press: New York, 1967.
29. Huang S, Fang YY, Lü AX, Lu GF, Ou ZP and Kadish KM. *J. Porphyrins Phthalocyanines* 2012; **16**: 958–967.
30. Kadish KM. In *Progress in Inorganic Chemistry*, Vol. 34, Lippard SJ. (Ed.) John Wiley & Sons: New York, 1986; pp 435–590.
31. Steene E, Dey A and Ghosh A. *J. Am. Chem. Soc.* 2003; **125**: 16300–16309.
32. Ghosh A and Steene E. *J. Inorg. Biochem*. 2002; **91**: 423–436.

33. Gao Y, Liu J, Wang M, Na Y, Åkermark B and Sun L. *Tetrahedron* 2007; **63**: 1987–1994.
34. Fryxelius J, Eilers G, Feyziyev Y, Magnuson A, Sun L and Lomoth R. *J. Porphyrins Phthalocyanines* 2005; **9**: 379–386.
35. Fuhrhop JH. *Struct. Bonding (Berlin)* 1974; **18**: 1–67.
36. Gouterman MJ. *Mol. Spectrosc*.1961; **6**: 138–163.
37. Perrin MH, Gouterman M and Perrin CL. *J. Chem. Phys*. 1969; **50**: 4137–4150.